



OPEN ACCESS

EDITED BY

Guoliang Qiao,
Massachusetts General Hospital and
Harvard Medical School, United States

REVIEWED BY

Jiang Chen,
Zhejiang University, China
Bernd Heinrich,
National Institutes of Health (NIH),
United States
Yona Keisari,
Tel Aviv University, Israel

*CORRESPONDENCE

Liping Xu
zlyyxulinping1475@zzu.edu.cn

[†]These authors have contributed
equally to this work

SPECIALTY SECTION

This article was submitted to
Gastrointestinal Cancers: Hepato
Pancreatic Biliary Cancers,
a section of the journal
Frontiers in Oncology

RECEIVED 13 June 2022

ACCEPTED 23 August 2022

PUBLISHED 08 September 2022

CITATION

Xu L, Yan M, Long J, Liu M, Yang H and
Li W (2022) Identification of
macrophage correlated biomarkers to
predict the prognosis in patients with
intrahepatic cholangiocarcinoma.
Front. Oncol. 12:967982.
doi: 10.3389/fonc.2022.967982

COPYRIGHT

© 2022 Xu, Yan, Long, Liu, Yang and Li.
This is an open-access article
distributed under the terms of the
[Creative Commons Attribution License
\(CC BY\)](https://creativecommons.org/licenses/by/4.0/). The use, distribution or
reproduction in other forums is
permitted, provided the original
author(s) and the copyright owner(s)
are credited and that the original
publication in this journal is cited, in
accordance with accepted academic
practice. No use, distribution or
reproduction is permitted which does
not comply with these terms.

Identification of macrophage correlated biomarkers to predict the prognosis in patients with intrahepatic cholangiocarcinoma

Liping Xu^{1*†}, Meimei Yan^{2,3†}, Jianpeng Long⁴,
Mengmeng Liu^{2,3†}, Hui Yang⁵ and Wei Li⁶

¹Department of Research and Foreign Affairs, The Affiliated Cancer Hospital of Zhengzhou University and Henan Cancer Hospital, Zhengzhou, China, ²Department of Hematology, The Affiliated Cancer Hospital of Zhengzhou University and Henan Cancer Hospital, Zhengzhou, China, ³Academy of Medical Sciences of Zhengzhou University, Zhengzhou, China, ⁴Department of Breast and Thyroid Surgery, Gansu Provincial Central Hospital, Lan Zhou, China, ⁵Department of Gastroenterology, Zhengzhou University People's Hospital and Henan Provincial People's Hospital, Zhengzhou, China, ⁶Department of Hematology, The First Affiliated Hospital of Zhengzhou University, Zhengzhou, China

Background: It has been shown that tumor-associated immune cells, particularly macrophages, play a fundamental role in the development and treatment response of intrahepatic cholangiocarcinoma (ICC). However, little is known about macrophages at the single cellular level of ICC patients.

Methods: ScRNA-seq from Zhang et al. was used in the present study to identify the genes differentially expressed in ICCs. Furthermore, transcriptomic data from TCGA datasets, IHC and flowcytometry from our cohort were used to confirm the findings. Kaplan-Meier and TIDE scores were also used for prognostic analysis and ICB responses.

Results: A significant number of macrophages were found in ICCs as compared to adjacent tissues. We then extracted, processed, and classified the macrophages from the ICCs and adjacent tissues into 12 clusters. Significantly, the macrophages from the ICC exhibited an immunosuppressed state in terms of both signature gene expression and functional enrichment. Furthermore, our results indicate that, of the 10 selective tumor-promoting genes of macrophages, only MMP19 and SIRP α can predict ICB responses in ICCs. Although a higher expression of MMP19 and SIRP α predict a poor prognosis for ICCs without immunotherapy after surgery, patients with high SIRP α expression were more sensitive to immunotherapy, whereas those with high MMP19 expression were not sensitive to immunotherapy. To define the mechanisms, we found that SIRP α ^{hi} ICCs exhibited an increased enrichment KEGG pathway of leukocyte transendothelial migration and neutrophil extracellular trap formation. The increased immune cell infiltration will increase sensitivity to immunotherapy.

Conclusion: Collectively, macrophages are critical to the immune status of ICCs, and MMP19 and SIRP α can predict prognosis and ICB responses for ICCs.

KEYWORDS

intrahepatic cholangiocarcinoma, immune cells, macrophages, SIRP α , MMP19

Introduction

Intrahepatic cholangiocarcinoma (ICC) is an aggressive and invasive cancer that arises in the liver, which accounts for the second most common cause of liver cancer worldwide (1, 2). There have been an increasing number of ICC cases and deaths over the last decade, causing concern globally (3). The only potentially curative treatment for patients with resectable ICC is surgery (4, 5). Despite liver resections being undertaken as a curative procedure, the 5-year survival rate of patients with liver resections is disappointing, with a 20% to 35% survival rate (4). In addition, since the onset of ICC is so insidious, most patients by the time of diagnosis have already reached a stage of advanced or metastatic cancer, and only a small proportion of tumors are resectable (3, 6). Adjuvant therapies, such as systemic chemotherapy and radiotherapy, are still poorly defined and have been reported to be only modestly effective (7, 8). The clinical effectiveness of immunotherapy and targeted therapies for patients with ICC remains ineffective, despite significant progress in both fields (9). It is therefore important to understand the immune microenvironment of ICCs for effective diagnosis and treatment.

Tumor tissue consists of tumor cells and tumor stroma. The tumor stroma is composed of both immune and non-immune stromal cells, which together form a complex microenvironment that promotes tumor growth (10). Drug development targeting the tumor microenvironment (TME) is a promising approach to treating many forms of cancer, and it is especially relevant to ICCs (11). In 2020, Zhang et al. first described the cellular dissection of ICCs and showed that the cellular landscape of ICCs exhibits a high level of diversity of malignant, immune and stromal cells (12). In their study, Zhang et al (12) characterized distinct populations of immune and stromal cells, in particular tumor-infiltrating lymphocytes (TILs) and cancer-associated fibroblasts (CAFs) in the context of a wide inter- and intra-tumor heterogeneity that also involve malignant cholangiocytes, as has

been anticipated by several studies conducted on ICCs (13). Miao Su et al. established nine-prognosis-related-genes (PRGs) by reanalyzing the scRNA-seq (14). These genes included SLC16A3, BNIP3L, TPM2, CLEC11A, EREG, PMAIP1, CEBPB, A2M, and TUBA1B, which are correlated with ICC prognosis (14). Studies show that macrophages are primarily responsible for regulating immune functions, hematopoiesis, metabolism, tissue repair, and maturation of embryonic tissue (15–19). However, the prognostic genes expressed by macrophages in ICCs, still has to be further investigated.

In this study, single-cell sequencing data, transcriptome sequencing data from the TCGA database, and flow cytometric analysis and immunohistochemical validation of ICC from our own unit were used to investigate in depth the prognostic role of altered immune cell subpopulations, particularly genes heterogeneously expressed by macrophages. In ICCs, we observed an increase in macrophages that are crucial for ICC development. An analysis of differentially expressed genes revealed that the macrophages in ICCs predominantly exhibited an immunosuppressive phenotype, whereas macrophages in tissues adjacent to the cancer predominantly exhibited an immune activating phenotype. Furthermore, MMP19^{hi} ICCs predict poorer response to ICB treatment and shorter DFS and OS compared with MMP19^{low} ICCs. Although the patients with SIRP α ^{hi} ICCs respond better to ICB treatment, those with SIRP α ^{hi} ICCs without immunotherapy had a shorter DFS and OS compared with SIRP α ^{low} ICCs, which indicates that patients with SIRP α ^{hi} should receive ICB treatment. Transcriptome sequencing explains the underlying molecular mechanisms of these two different biomarkers in predicting differences in ICB treatment response. Our study highlights that macrophage plays an important role in the progression of ICCs, and targeting macrophage therapy may be a new and effective approach in immunotherapy.

Materials and methods

ScRNA-seq database

The scRNA-seq datasets of ICC cells and paracancer tissue cells were acquired from the Gene Expression Omnibus (GEO) database (GSE138709, GSE142784), and the 10X Genomic

Abbreviations: CAFs, Cancer-associated fibroblasts; CTLA4, cytotoxic T-lymphocyte-associated protein 4; GDF15, Growth differentiation factor 15; GEO, Gene Expression Omnibus; ICC, Intrahepatic cholangiocarcinoma; PD-1, Programmed death 1; PD-L1, programmed death-ligand 1; QC, Quality control; TILs, Tumor-infiltrating lymphocytes; TME, Tumor microenvironment.

scRNA-seq data was acquired from five ICC samples and three adjacent tissues reported by Zhang et al. (12). The information regarding the cell preparation and single-cell transcriptome profiling is described in the original paper (12).

Quality control and data processing

We combined single-cell data from ICC patients and healthy donors using the merge function found in version 3.2.2 of the Seurat R package, as previously described (20). Briefly, the cells that have unique feature counts of $> 3,000$, < 200 and $\geq 10\%$ mitochondrial counts were filtered. The merged dataset was normalized using the Seurat “NormalizedData” function, with a global scaling normalization method “LogNormalize,” and this was multiplied by a scale factor (10,000 by default). It was then scaled by performing the Seurat “ScaleData” function, with regression of the variation of “nCount_RNA” and “percent.mt.” Performing the Seurat “JackStrawPlot” and “ElbowPlot” functions aided in the selection of suitable dimensionality. Dimension reduction analysis was performed with the Seurat “RunPCA” function, and non-linear dimensional reduction was performed with the Seurat “RunUMAP” function. The tSNE analysis was used for dimension reduction to determine the cell populations and for visualization of the gene expression (14). The FindClusters function was performed with a resolution of 0.5, and the RunTSNE function was used to generate clusters. The FindAllMarkers function (arguments: min.pct = 0.25, logfc.threshold = 0.25) was used to find markers by comparing each cluster to all others, and different genes between two identities were identified with the FindMarkers function. The feature plot and heatmap visualization of gene expression were generated using the Seurat functions FeaturePlot and DoHeatmap, respectively (14). Clusters consisting of macrophages were extracted and processed again as described above, and each macrophage type was further divided into subclusters. Marker genes of each macrophage type were identified by comparing ICC subclusters with adjacent subclusters, and adjustment of P-value ($\text{adjPval} < 0.05$) was regarded as the cutoff criteria. The marker genes of each macrophage type were incorporated as differentially expressed genes (DEGs). Finally, macrophages from tumor tissue were extracted and processed again as described above. Differences in pathway activity were analyzed by a gene set variation analysis (GSVA) (12).

Single cell suspension preparation and flow cytometry

The freshly resected surgical ICCs and adjacent tissue samples from our cohort were immediately washed with phosphate-buffered saline (PBS) and processed to generate

single cell suspensions for the subsequent flow cytometry. Tissue digestion was performed in 15 ml tubes containing 10 ml pre-warmed RPMI 1640 (ThermoFisher Scientific) with trypsin, 1 mg/ml type IV collagenase (Sigma) and 10 U/ μl DNase I (Roche) at 37°C for 30 minutes. The reaction was deactivated with 10% FBS. Cell suspensions were filtered using a 70 μM filter and then centrifuged at 500 rpm at 4°C for 6 min to pellet dead cells and red blood cells. The cells were washed twice and suspended in PBS with 0.5% bovine serum albumin (BSA, Sigma). Thereafter, the concentration of the single cell suspension was calculated, and 5×10^6 cells were taken for subsequent flow cytometry assays, as previously described (18, 21, 22). The flow cytometry method was used to analyze the macrophage percentage by staining with anti-human APC-Cy7-CD45 (Biolegend, Cat#:304014, 0.1 $\mu\text{l}/10^6$ cells), anti-human Percp-CD14 (Biolegend, Cat#: 325632, 0.1 $\mu\text{l}/10^6$ cells) and anti-human PE-Cy7-CD16 (Biolegend, Cat#: 302015, 0.1 $\mu\text{l}/10^6$ cells). After blocking, cells from ICC and adjacent tissues were stained with anti-human APC-Cy7-CD45, anti-human Percp-CD14 and anti-human PE-Cy7-CD16 on ice for 30 minutes in the dark. After staining, the cells were washed once with PBS plus 0.5% BSA and 2 mM EDTA. DAPI were used to gate out dead cells, and then the cells were resuspended in PBS plus 0.5% BSA and 2mM EDTA and run on a BD Air III (BD bioscience). Flow Jo software (BD) was used to analyze the data.

ICC samples, follow-up and survival analysis

Twenty ICC and 20 adjacent tissue samples were obtained from patients who underwent curative resection of ICCs between October 1, 2016 and October 1, 2019 at the Affiliated Cancer Hospital of Zhengzhou University. This study was approved by the Ethics Committee at the Affiliated Cancer Hospital of Zhengzhou University. All methods and procedures associated with this study were conducted in accordance with the Good Clinical Practice guidelines and aligned with the ethical principles of the Declaration of Helsinki as well as local laws. All enrolled patients were pathologically diagnosed with ICCs and did not receive any anti-cancer treatments before surgery. Follow-up and survival analysis of ICC patients were consistent with methods used in previous studies (23, 24). After surgery, the patients were checked regularly. During the first two years, follow-up evaluations were measured every 3 months. During the 2 to 5 year period after surgery, the follow-up tests of ICC patients were examined every 6 months, and, beyond 5 years, they were measured every year. The follow-up tests included complete blood examinations, tumor biomarkers and chest and abdominal computed tomography scans. If follow-up evaluations revealed metastatic disease and/or local recurrences, other therapies were applied, including

conventional therapies (surgery, chemotherapy, and radiotherapy) as well as targeted and immunotherapy. Disease-free survival (DFS) was calculated from the date of surgery to the time of recurrence or metastasis, and patients who were alive and in a stable state were censored at the time of last contact (25–27). Overall survival (OS) was calculated from the date of surgery to the time of death, and patients who were alive at the time of last contact were censored (25–27). DFS and OS were calculated using the Kaplan–Meier analysis. The final follow-up was performed on January 1, 2022.

IHC staining and quantitative analysis

Formalin-fixed and paraffin-embedded sections of intrahepatic cholangiocarcinoma tissue (N=20) and paracancerous tissue (N=20, 5µm thick) from our cohort were dewaxed and rehydrated. Antigen retrieval was performed by heating the slides in 10 mM Tris buffer with 1 mM EDTA (pH 9) in a steamer for 20 min. Inhibition of endogenous peroxidase activity was achieved by immersion in 3% H₂O₂ for 5 minutes. After washing the tissue with Tris-buffered saline (TBS) containing Tween, endogenous biotin was inhibited through sequential incubation with 0.1% anti-biotin protein and 0.01% biotin (Dako, Glostrup, Denmark), respectively, at room temperature for 10 min. Other non-specific binding sites were blocked with 3% skimmed milk powder at room temperature for 30 minutes. The ICC and paracancerous tissue sections were incubated with the monoclonal mouse antibody anti-human CD68 (Abcam, Cat# ab213363), SIRPα (Abcam, Cat# ab260039), and MMP19 (Abcam, Cat# ab53146) at 4 °C for one night. Subsequently, the sections were serially rinsed and incubated with secondary antibodies. The immunohistochemical staining was evaluated independently by two experienced pathologists, who were blinded to the patients' clinical characteristics and outcomes. H-score was used to quantify the expression of CD68, SIRPα, and MMP19 as previously described (28). The median was selected as the cutoff value for high or low CD68, SIRPα and MMP19 expression.

TCGA datasets

The Limma package (version 3.40.2) of R software was used to study the differential expression of mRNAs (29). The adjusted *P*-value was analyzed to correct for false positive results in TCGA or GTEx. “Adjusted *P* < 0.05 and Log₂ (Fold Change) > 1 or Log₂(Fold Change) < −1” were defined as the thresholds for the screening of differential mRNA expression. Raw counts of RNA-sequencing data of 36 ICC patients from TCGA datasets were used to analyze the differentially expressed genes, based on the high and low expression of selective genes. To further confirm the underlying function of the potential targets, the

data was analyzed *via* functional enrichment. The Kyoto Encyclopedia of Genes and Genomes (KEGG) Enrichment Analysis is a practical resource for the analytical study of gene functions and associated high-level genome functional information. To better understand the carcinogenesis of mRNA, the ClusterProfiler package (version: 3.18.0) of R was employed to analyze the enrichment of the KEGG pathway as our previous described (26).

ICB responses analysis

Raw counts of RNA-sequencing data and corresponding clinical information from 36 ICC patients were obtained from TCGA dataset (<https://portal.gdc.cancer.gov/>), with methods of acquisition and application that comply with the guidelines and policies. Potential ICB response was predicted with a TIDE algorithm, as our and other authors previously described (26, 30). Using gene expression markers, TIDE provides insight into two different mechanisms of tumor immune escape, namely dysfunction of tumor-infiltrating cytotoxic T lymphocytes (CTL) and exclusion of CTL by immunosuppressive factors. It has been shown that high TIDE scores are associated with poor immuncheckpoint blockade therapy (ICB) efficacy and short survival following ICB treatment (26). Therefore, TIDE score is a novel method for predicting ICB responses.

Statistical analysis

GraphPad Prism 9.0 software (GraphPad Software, Inc.) was used to perform the statistical analysis. Quantification of CD68, SIRPα, and MMP19 density and CD14 and CD16 percentage were analyzed *via* a *t*-test. The DFS and OS were calculated using the Kaplan-Meier estimator. *P* < 0.05 was used to indicate a statistically significant difference for all data.

Results

ScRNA-seq characterization of the immunomicroenvironment of human ICCs

The TME is formed by tumor cells, tumor-associated fibroblasts, and the surrounding tissues, immune cells, blood vessels and extracellular matrix, and other elements. In the present study, we investigated the TME of ICC patients by 10X Genomics sequencing from the GEO database (12). The quality control chart shows the detected gene number range, UMI count for each cell and the percentage of mitochondrial genes (Supplementary Figures 1A–G). In the original paper, the

cells were classified into 10 distinct cell types, using known marker genes (12). To further cluster the cells precisely, the samples were successfully classified into 23 clusters with the t-distributed stochastic neighbor embedding (t-SNE) algorithm. Based on the expression of canonical and functional marker genes, these clusters included the following (Figure 1A and Supplementary Table 1):

- Cluster 0 (CD8⁺T/NKT/NK cells, marked with CD3E, CD8A, GZMA, GZMH, CD69, KLRB1, IL32 and CCL5, Supplementary Figure 2),
- Cluster 1 (S100^{hi} malignant cells, marked with S100A2, AKR1C2, S100A6, S100A10, S100A16, S100A14 and KRT7, Supplementary Figure 8),
- Cluster 2 (CD7⁺ T cells, malignant cells, marked with DUSP2, CREM, CD7 and CXCR4, Supplementary Figure 2),
- Cluster 3 (ITGA^{hi} malignant cells, marked with PMEPA1, ITGA2, ITGA3 and KRT19 Supplementary Figure 8),
- Cluster 4 (FGG^{hi} cholangiocytes, marked with FGG, DEFB1, CLU, TM4SF4 and AKR1C3, Supplementary Figure 7),
- Cluster 5 (RNASE1^{hi} endothelial cells, marked with RAMP2, RNASE1, CCL2 and CLEC14A Supplementary Figure 6),
- Cluster 6 (GDF15^{hi} cholangiocytes, marked with GDF15, CAPS and ANXA4, Supplementary Figure 7),
- Cluster 7 (ACTA2^{hi} fibroblasts, marked with ACTA2, TAGLN, MYL9 and NDUFA4L2, Supplementary Figure 5),
- Cluster 8 (IL1B^{hi} macrophages, marked with S100A8, S100A9, IL1B, AIF1, CD68 and LYZ, Supplementary Figure 4),
- Cluster 9 (A2M^{hi} endothelial cells, marked with CLDN5, A2M, VWF, CD34 and RAMP2, Supplementary Figure 6),

- Cluster 10 (HLA^{hi} macrophages, marked with HLA-DPB1, HLA-DQA1, HLA-DQA1, HLA-DRB1 and CD74, Supplementary Figure 4),
- Cluster 11 (MKI67^{hi} NK cells, marked with MKI67, HMGB2, GZMA, NKG7 and GZMB, Supplementary Figure 3),
- Cluster 12 (COL1A1^{hi} fibroblasts, marked with COL1A1, COL3A1, DCN, IGFBP7 and CCL2, Supplementary Figure 5),
- Cluster 13 (AKR1C2^{hi} malignant cells, marked with AKR1C2, KRT7 and HMGA1, Supplementary Figure 8),
- Cluster 14 (SLC40A1^{hi} macrophages, marked with C1QA, C1QB, C1QC, APOE, FCGR3A and SLC40A1, Supplementary Figure 4),
- Cluster 15 (CD79A^{hi} B cells, marked with CD79A, MZB1, IGJ, DERL3 and CD79B, Supplementary Figure 3),
- Cluster 16 (DNASE1L3^{hi} endothelial cells, marked with DNASE1L3, CD36, PPAP2B, AKAP12 and RAMP3, Supplementary Figure 6),
- Cluster 17 (RBP1^{hi} malignant cells, marked with RBP1, FN1, ANXA2 and KRT7, Supplementary Figure 8),
- Cluster 18 (TM4SF4^{hi} cholangiocytes, marked with TM4SF4, ANXA4 and DEFB1, Supplementary Figure 7),
- Cluster 19 (APOC1^{hi} hepatocytes, marked with ALB, MT1G and APOC1, Supplementary Figure 7),
- Cluster 20 (CD27^{hi} B cells, marked with SLAMF7, CD27, CD79A and MZB1, Supplementary Figure 3),
- Cluster 21 (PDGFRB^{hi} endothelial cells, marked with NDUFA4L2, PDGFRB, RAMP2 and TAGLN, Supplementary Figure 6),
- Cluster 22 (MKI67^{hi} macrophages, marked with MNDA, MKI67 and SPI1, Supplementary Figure 3).

More marker genes of each cluster are demonstrated in Figure 1B and Supplementary Table 1, which confirmed the accuracy of cell identity. In addition, the cells derived from the ICC or control tissues are shown in Figure 1C. This data demonstrated that Clusters 0, 2, 10, 11, 16, 18 and 19 were from the control tissues, and, in contrast, Clusters 1, 3, 4, 5, 6, 7, 8, 9, 12, 13, 14, 15, 17, 20, 21 and 22 were from the cancer tissues.

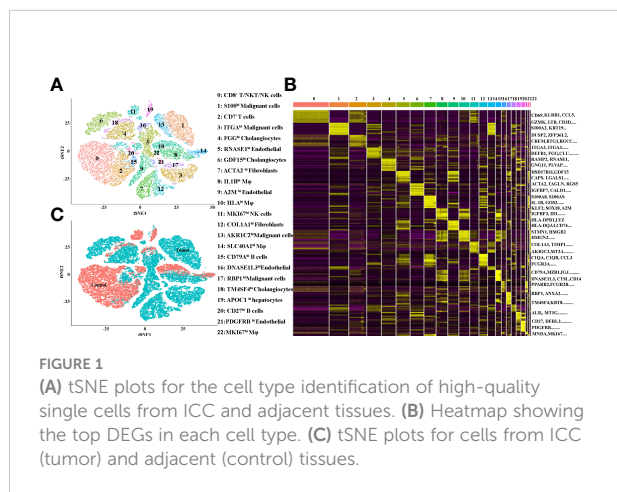
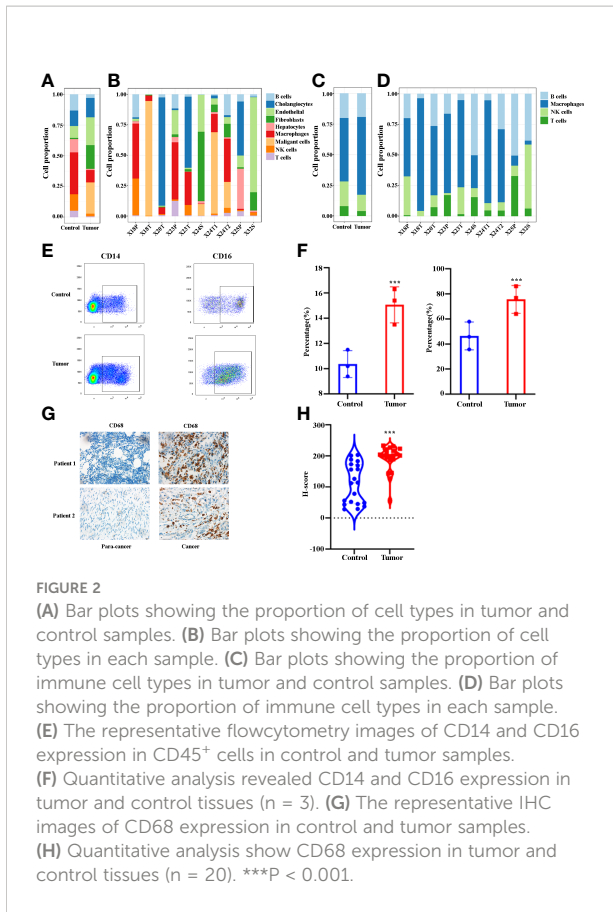


FIGURE 1 (A) tSNE plots for the cell type identification of high-quality single cells from ICC and adjacent tissues. (B) Heatmap showing the top DEGs in each cell type. (C) tSNE plots for cells from ICC (tumor) and adjacent (control) tissues.

Macrophages increased in the microenvironment of human ICCs

In order to better understand immune cell infiltration in human ICC, we first analyzed the cell proportion of all cell types in the control and the tumor tissue. Figure 2A demonstrates that B cells, hepatocytes, macrophages, NK cells and T cells in tumor samples decreased compared with the control samples. The proportion of each cell type varied greatly by sample (Figure 2B), which suggests the heterogeneity of the ICC samples.

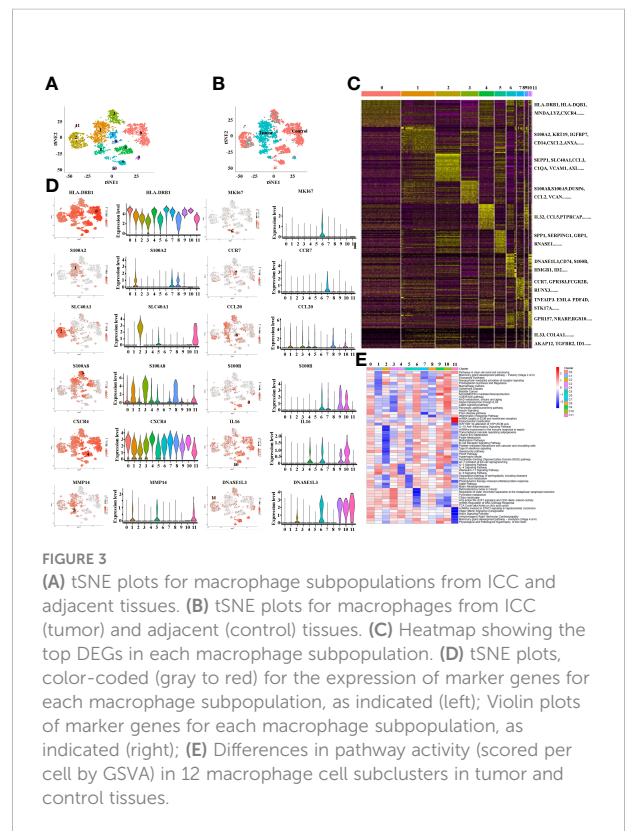


We then analyzed the immune cell proportion in the control and tumor tissue. As shown in **Figure 2C**, macrophages are the only immune cells to increase. Remarkably, the macrophage subclusters were highly patient-specific (**Figure 2D**), suggesting the heterogeneity of macrophages in ICC patients. Thereafter, we investigated the changes in macrophages in ICC by staining CD14 and CD16. **Figure 2E** shows representative flowcytometry images of CD14 and CD16 of paracancer and cancer tissues. A quantitative analysis revealed that the CD14⁺ and CD14⁺CD16⁺ increase significantly (**Figure 2F**). We next examined the total macrophage percentage in the paracancer and cancer tissues by staining total macrophage marker CD68 by IHC. **Figures 2G, H** demonstrate that CD68 increases significantly in ICC patients. Collectively, our findings demonstrate that macrophages, especially CD14⁺CD16⁺ subclusters, are increased in the microenvironment of ICCs.

Immunosuppressive tumor-associated macrophages enriched in human ICC tumors

Tumor-infiltrating immune cells are highly heterogeneous and have been shown to play important roles in immune evasion

and the response to immunotherapy treatment (31). In the present study, the total macrophages from cancer and paracancer tissue were extracted, and they exhibited 12 distinct subclusters (**Figure 3A**). The tSNE plot shows the subcluster distribution among the sample pathology (**Figure 3B**). As illustrated in **Figures 3A, B**, Clusters 1, 5 and 9 were defined from cancer tissues, while the other clusters were from paracancer tissue. A heatmap of the top 30 marker genes for each cluster is shown in **Figure 3C**. All marker genes of these 12 clusters are demonstrated in **Supplementary Table 2**. According to the differentially expressed genes, the macrophages were designed as Cluster 0: HLA⁺, Cluster 1: S100A2⁺, Cluster 2: SLC40A1⁺, Cluster 3: S100A8⁺, Cluster 4: CXCR4⁺, Cluster 5: MMP14⁺, Cluster 6: MKI67⁺, Cluster 7: CCR7⁺, Cluster 8: CCL20⁺, Cluster 9: S100B⁺, Cluster 10: IL16⁺ and Cluster 11: DNASE1L3⁺ (**Figure 3D** and **Supplementary Table 2**). In addition, we found that macrophage subpopulations (clusters 1, 5, 7, 8, and 9) from cancer tissues expressed a certain number of immunosuppressive genes, such as VEGFA, MMP14, MMP19, S100A2, APOE, HMOX1, SLAMF7, SIRPα, LAG3 and IL18. In contrast, macrophage subpopulations (clusters 0, 2, 3, 4, 6, 10 and 11) from paracancer tissues are characterized by the prominent expression levels of activated markers such as HLA-DRB1, HLA-DQB1, HLA-DQA1, HLA-DPB1, HLA-DPA1, CD74, MNDA, CXCR4, CCR7, GPR183, IL32, CCL5 and IL16. Based on the marker genes, the GO terms enriched in



findings revealed different macrophage subpopulations and a highly heterogeneous immune microenvironment that improves our understanding of ICC pathogenesis.

Immune checkpoint blockade responses analysis based on selective tumor-promoting genes of TAMs in ICC

Programmed death 1 (PD-1), programmed death-ligand 1 (PD-L1) and cytotoxic T-lymphocyte-associated protein 4 (CTLA4) monoclonal antibodies are currently the most prominent targets for immunotherapy in ICCs, yet approximate one-third of patients have been found to respond to immunotherapy in clinical use (9). Tumor immune dysfunction and exclusion (TIDE) is a sufficient approach to predict the ICB response (30). We investigated the ICC patients' response to the ICB, based on selective immunosuppressive genes of TAMs from TCGA dataset. Our results indicated that, of the selective 10 tumor-promoting genes of TAMs, only MMP19 (Figure 6A), and SIRPα (Figure 6B) can predict ICB response in ICC patients. Interestingly, lower ICB responses are predicted for MMP19^{hi} ICC patients, compared with MMP19^{low}

patients (Figure 6A). In contrast, higher ICB responses are predicted for SIRPα^{hi} ICC patients, compared with SIRPα^{low} patients (Figure 6B). Furthermore, there are no significant ICB response predictions with high and low TIDE score groups of VEGFA (Figure 6C), MMP14 (Figure 6D), S100A2 (Figure 6E), APOE (Figure 6F), HMOX1 (Figure 6G), SLAMF7 (Figure 6H), LAG3 (Figure 6I) and IL18 (Figure 6J).

The expression of MMP19 and SIRPα significantly increased in ICC patients and predict poor overall survival time with high expression

Having shown that MMP19 and SIRPα can predict the ICB responses, we proceeded to confirm the expression of MMP19 and SIRPα by IHC between ICC and paracancer tissues. Twenty ICC and 20 paracancer tissue samples collected between July 1, 2016 and July 1, 2019 from The Affiliated Cancer Hospital of Zhengzhou University were tested for the expression of MMP19 and SIRPα. All the patients had undergone surgery and were not treated with immunotherapies during the treatment process until death. At the last contact (December 31, 2021), all the patients were deceased. Figure 7A indicated the expression of MMP19 on macrophage

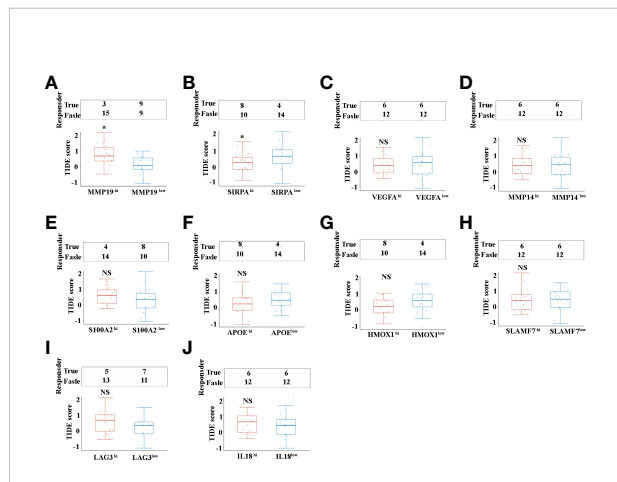


FIGURE 6 (A) The ICB response score (TIDE score) between MMP19^{hi} and MMP19^{low} ICC from 36 TCGA samples. (B) The ICB response score (TIDE score) between SIRPα^{hi} and SIRPα^{low} ICC from 36 TCGA samples. (C) The ICB response score (TIDE score) between VEGFA^{hi} and VEGFA^{low} ICC from 36 TCGA samples. (D) The ICB response score (TIDE score) between MMP14^{hi} and MMP14^{low} ICC from 36 TCGA samples. (E) The ICB response score (TIDE score) between S100A2^{hi} and S100A2^{low} ICC from 36 TCGA samples. (F) The ICB response score (TIDE score) between APOE^{hi} and APOE^{low} ICCs from 36 TCGA samples. (G) The ICB response score (TIDE score) between HMOX1^{hi} and HMOX1^{low} ICC from 36 TCGA samples. (H) The ICB response score (TIDE score) between SLAMF7^{hi} and SLAMF7^{low} ICC from 36 TCGA samples. (I) The ICB response score (TIDE score) between LAG3^{hi} and LAG3^{low} ICC from 36 TCGA samples. (J) The ICB response score (TIDE score) between IL18^{hi} and IL18^{low} ICC from 36 TCGA samples. *P < 0.05, NS, no significant difference.

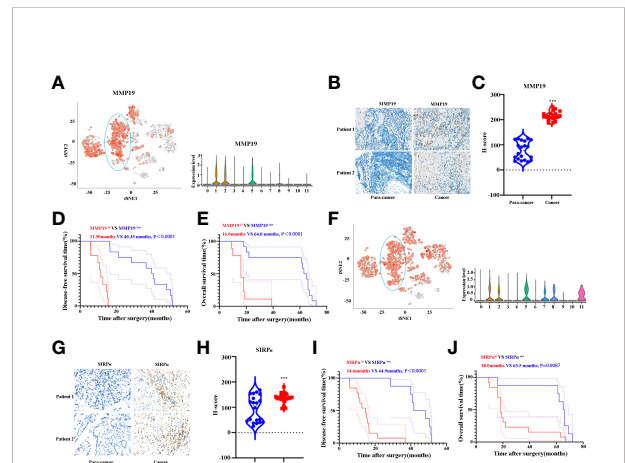


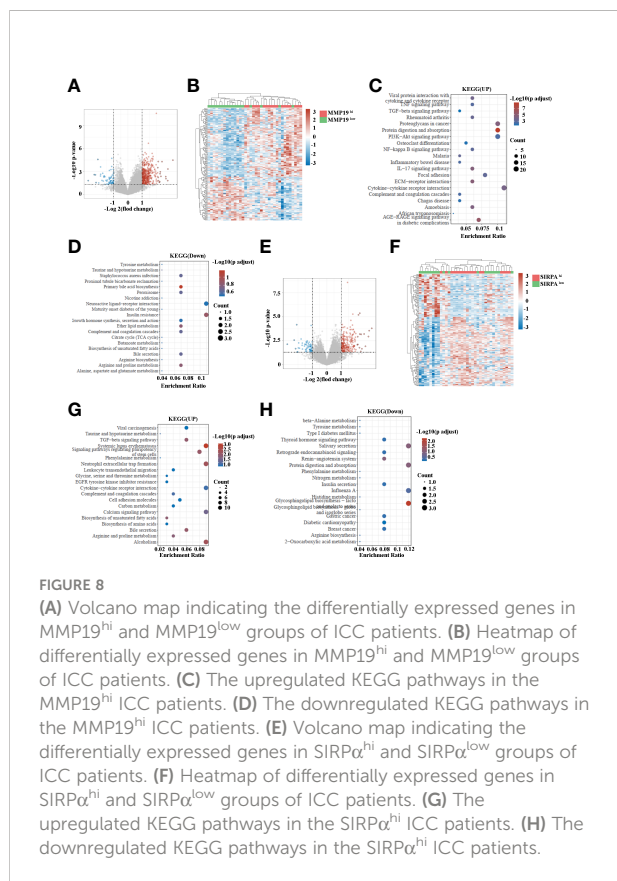
FIGURE 7 (A) tSNE plots, and Violin plots for the expression of MMP19 for macrophage subpopulations. (B) The representative IHC images of MMP19 expression in control and tumor samples. (C) Quantitative analysis revealed MMP19 expression in tumor and control tissues (n = 20). (D) The DFS curves of ICC patients based on the high and low expression of MMP19. (E) The OS curves of ICC patients based on the high and low expression of MMP19. (F) tSNE plots, and Violin plots for the expression of SIRPα for macrophage subpopulations. (G) The representative IHC images of SIRPα expression in control and tumor samples. (H) Quantitative analysis revealed SIRPα expression in tumor and control tissues (N = 20). (I) The DFS curves of ICC patients based on the high and low expression of SIRPα. (J) The OS curves of ICC patients based on the high and low expression of SIRPα. ***P < 0.001.

subclusters from ICC and paracancer tissue by Sc-RNA-seq. Figures 7B, C demonstrate that the expression of MMP19 increased significantly in ICC compared to the paracancer tissue. A Kaplan–Meier analysis indicated that MMP19^{hi} patients had a shorter DFS (Figure 7D) and OS (Figure 7E) compared with MMP19^{low} patients. Using the same method, we showed the expression of SIRP α on macrophage subclusters from ICC and paracancer tissue by Sc-RNA-seq (Figure 7F). And we confirmed that SIRP α increased significantly in ICC tissue (Figures 7G, H). The Kaplan–Meier analysis revealed that SIRP α ^{hi} patients had a shorter DFS (Figure 7I) and OS (Figure 7J) than SIRP α ^{low} patients. Collectively, higher expression of MMP19 and SIRP α predict a poor prognosis for ICC patients after surgery.

Transcriptome analysis of ICC tissue based on the high and low expression of MMP19 or SIRP α

Having shown that MMP19^{hi} expression predicts a poor response to ICB treatment, while SIRP α ^{hi} expression predict a better response to ICB treatment in ICC patients, we analyzed the transcriptome data of MMP19^{hi} and MMP19^{low} ICC tissues. A total of 495 genes were distinguished as differentially expressed mRNAs, with 431 genes upregulated and 64 genes downregulated

(Figures 8A, B and Supplementary Table 4). The selective upregulated genes in MMP19^{hi} patients included MMP12, MMP7, VCAM1, IL6, GAS7, CXCL5, CXCL13, CCL21, CCL18 and S100A1. Figure 8C shows the enrichment of KEGG pathways in the MMP19^{hi} group, including focal adhesion, ECM-receptor interaction, the IL17 signaling pathway, the TNF signaling pathway, the TGF-beta signaling pathway and cytokine-cytokine receptor interaction. The downregulated KEGG pathways in the MMP19^{hi} group included the primary bile acid biosynthesis, insulin resistance, bile secretion and biosynthesis of unsaturated fatty acids (Figure 8D). We next analyzed the transcriptome differences between SIRP α ^{hi} and SIRP α ^{low} ICCs with the same method. A total of 296 genes were distinguished as differentially expressed mRNAs, with 234 genes upregulated and 62 genes downregulated (Figures 8E, F and Supplementary Table 5). The selective upregulated genes in SIRP α ^{hi} patients included IGFBP1, APOA2, ALB, TFR2, SLC23A1, CDH6, TNFSF15, APOB, GDF15, SLC17A1, SLC17A3, SLC28A1, SLC39A5, SLC27A2, CXCL8, SLC40A1, CXCL12, TGF-B2, CCL2 and CXCL6 (Supplementary Table 5). Figure 8G shows the enrichment of KEGG pathways in the SIRP α ^{hi} group, including cell adhesion molecules, the calcium signaling pathway, biosynthesis of unsaturated fatty acids, bile secretion, biosynthesis of amino acids, leukocyte transendothelial migration and neutrophil extracellular trap formation. The downregulated KEGG pathways in the SIRP α ^{hi} group included nitrogen metabolism, insulin secretion and histidine metabolism (Figure 8H).



Discussion

A growing body of research has revealed that a deeper understanding of the TME, in particular the characterization of tumor-infiltrating immune cells, is essential for exploring key regulatory molecules in tumor development and immunotherapy (11, 32, 33). Using 10X genomic single-cell sequencing, Zhang et al. report the first complete subpopulation of cholangiocarcinoma immune microenvironment cells (12). The study identified six distinct subpopulations of fibroblasts, most notably vascular cancer-associated fibroblasts (vCAFs) that express microvascular signature genes. Therefore, the study focused on a novel cellular interaction between ICCs and vCAFs and identified potential targets for the treatment of ICC (12). Chen et al. (34) reanalyzed the Sc-RNAseq data and found that PNOC was mainly expressed by B cells in TME and could be an independent indicator for a better prognosis. LAIR2 was mainly expressed by Treg and partial CD8⁺/GZMB T cells, which could be an indicator of exhaustive T cell populations in TME. Both PNOC and LAIR2 were correlated with high immune infiltration levels in ICC patients (34). Miao Su et al. defined nine prognostic genes, including SLC16A3, BNIP3L, TPM2, CLEC11A, EREG, PMAIP1, CEBPB, A2M, and TUBA1B using the same Sc-RNAseq data (14). However, the roles of macrophages on the single-cell molecular profile in the prognosis

of patients with cholangiocarcinoma are still unclear. In the present study, we used Sc-RNaseq data, bulk sequencing data of cholangiocarcinoma patients in TCGA database, flowcytometry analysis and IHC analysis for an in-depth investigation of the immune phenotypes and macrophage subpopulations and their heterogeneity and roles in the prognosis of ICCs.

Significantly, in the original study of Zhang et al. (12), they did not fully investigate the function of macrophages. In the present study, we first examined immune infiltration in ICCs. The percentage of macrophages in the total number of immune cells increased significantly. The increased macrophage infiltration in ICCs was also confirmed by IHC, which is consistent with our previous study (25). Molecularly, macrophages can be divided into two types, namely M1- and M2-like macrophages and these cells are involved in anti-tumor activity and immunosuppressive tumor promotion (35, 36). Using fresh ICC and paracancer tissue, we found that the percentage of CD14⁺CD16⁺ macrophages (M2-like) had significantly increased in ICCs. Previous studies indicated that CD14⁺CD16⁺ macrophages can suppress T-cell activation in MM patients (37). While, the “M1-M2” macrophage dichotomy is too simple to describe their complicated roles in the TME (38). Significantly, not all tumor-promoting TAMs have M2-like phenotypes, thus highlighting the importance of defining TAM states beyond the M1/M2 dichotomy (39). Single-cell sequencing technology is an important method to study TAM heterogeneity (39). In the present study, we classified macrophages originating from tumor and paracancerous tissue into 12 subpopulations using ScRNA-seq. Clusters 1, 5 and 9 are mainly from ICC tissue, which expressed a number of tumor-promoting genes, such as VEGFA (40), MMP14 (41, 42), MMP19 (43), S100A2 (44), APOE (45), HMOX1 (46), SLAMF7 (47), SIRP α (25, 48), LAG-3 (49), and IL-18 (50). These biomarkers are correlated with poor prognosis of many types of cancers. In contrast, macrophage subpopulations (Clusters 0, 2, 3, 4, 6, 7, 8, 10 and 11) from paracancer tissues were characterized by prominent expression levels of immune activated markers, such as HLA-related molecules (HLA-DRB1, HLA-DQB1, HLA-DQA1, HLA-DPB1, HLA-DPA1 and CD74) (51), MNDA (52), CXCR4 (53), CCR7 (54), GPR183 (55), IL32 (56), CCL5 (57), and IL16 (58). Despite these findings, macrophages are extremely heterogeneous in ICCs. There is still a subpopulation of macrophages that overexpress antigen-presentation-related molecules HLA-DQA1, HLA-DRB1 and CD74 in patients with ICC. These results suggest that a “one-size-fits-all” approach to treating ICC by deleting macrophages is not a good treatment option. Clinical studies have also confirmed that deleting macrophages through CSF1R antibodies has poor clinical responses (59). Furthermore, Gloria H.Y. Lin et al. reported that disrupting CD47-SIRP α pathway triggers phagocytosis of cancer cells by all macrophage subpopulations, especially M1 and M2c macrophages (60). O’Connell P et al. found that elevated SLAMF7 expression was associated with T-cell depletion (61). And Chen J et al. found that patients with high SLAMF7 expression responded better to CD47-SIRP α blockade treatment compared with low

SLAMF7 expression (47). Our present study demonstrated that SIRP α and SLAMF7 highly expressed in ICCs compared with paracancer tissues. Collectively, these results suggest that ICC patients are sensitive to blocking CD47-SIRP α axis and that future clinical trials should be conducted to test this hypothesis.

ICB immunotherapy significantly improves the prognosis of patients with a wide range of tumors; however, only a minority of patients can benefit from ICB treatment (30). Several biomarkers or methods, such as PD-L1 (62), TMB (63), MSI (64) and MMR (65), have been reported to predict responses to ICB in multiple types of tumors. TIDE is a sufficient approach to predict the response to ICB (66). In the present study, we tested the 12 immunosuppressive genes in ICCs, and our results indicate that only MMP19 and SIRP α can predict the response to ICB. Interestingly, MMP19^{hi} ICCs showed poor responses to ICB treatment. In contrast, SIRP α ^{hi} ICCs demonstrated improved responses to ICB treatment. In addition, survival analysis revealed that MMP19^{hi} or SIRP α ^{hi} ICCs have a shorter OS. Transcriptome sequencing results showed that there are 431 upregulated genes and 64 downregulated genes in MMP19^{hi} ICCs. The upregulated enrichment of KEGG pathway in MMP19^{hi} ICCs included focal adhesion, ECM-receptor interaction, the IL17 signaling pathway, the TNF signaling pathway, the TGF-beta signaling pathway, and cytokine-cytokine receptor interaction, which can explain the poor response to ICB treatment, at least in part.

There is an interesting finding in ICCs with SIRP α ^{hi} that are not treated with immunotherapy resulting in a shorter OS, indicating that SIRP α is a negative prognostic marker for ICCs. However, increased expression of SIRP α is associated with stronger responses to ICB therapy, indicating that SIRP α ^{hi} ICCs require ICB therapy to extend OS. To explain the potential mechanisms, we performed a comparative analysis of transcriptomic data from ICC patients with high and low expression of SIRP α . The upregulated enrichment of KEGG pathways in the SIRP α ^{hi} group included leukocyte transendothelial migration and neutrophil extracellular trap formation. In general, increased tumor-infiltrating leucocytes can lead to a poorer prognosis when the patient is not receiving immunotherapy (66), because most immune cells in SIRP α ^{hi} ICCs have immunosuppressive phenotype. It is important to note, however, that the effectiveness of ICB treatment depends on the presence of tumor-infiltrating immune cells (67). CD47 acts as a “don’t eat me” signal that protects cells from phagocytosis by binding and activating its SIRP α receptor on macrophages (68). CD47 blockades or SIRP α fusion proteins direct targeting macrophages and significantly increase both innate and adaptive immunity against many types of cancer (68). Significantly, the effects of CD47 blockades or SIRP α fusion proteins depend on the presence of total macrophages (69). Both M1 and M2 macrophages are receptive to the action of CD47 monoclonal antibodies or SIRP α fusion proteins to exert their anti-tumor effects (60). Previous studies have indicated that both mouse and human TAMs express PD-1, and the expression

levels increase during the growth of cancer in mouse models and high TNM staging in primary human cancers (70). PD-1⁺ TAMs exhibit an M2-like macrophage phenotype and show a significantly reduced phagocytic potency against cancer cells (70). However, inhibition of the interaction between PD-1 and PD-L1 *via* either a PD-1 or a PD-L1 blockade leads to an anti-tumor immune response in mice that lacks T cells, B cells and NK cells but has functional macrophages (70). In conclusion, increased macrophage infiltration indicates a poor prognosis in the absence of immunotherapy, and these patients may be more sensitive to ICB therapy.

However, our study has limitations. We have only validated the expression of some biomarkers and their relationships with the prognosis of small samples of ICCs and immunotherapy. Nevertheless, macrophages continue to play an important role in the progression of ICCs, and targeting macrophage therapy may be a new and effective means of immunotherapy. Last, independent studies with larger sample size are required to confirm the findings of this study.

Data availability statement

The original contributions presented in the study are included in the article/**Supplementary Material**. Further inquiries can be directed to the corresponding author.

Ethics statement

This study was reviewed and approved by The Affiliated Cancer Hospital of Zhengzhou University. The patients/participants provided their written informed consent to participate in this study.

Author contributions

WL and LX designed, wrote, and edited the manuscript; analyzed the data; and finished the figures. HY, JL revised the

manuscript. MY and ML analyzed the data. All authors contributed to the article and approved the submitted version.

Funding

This study was supported by Key Research Projects of Henan Higher Education Institutions (21A320049) and Henan Province Medical Science and Technology Research Project (SBGJ202102063).

Acknowledgments

We thank all of the authors listed in this manuscript.

Conflict of interest

The authors declare that the research was conducted in the absence of any commercial or financial relationships that could be construed as a potential conflict of interest.

Publisher's note

All claims expressed in this article are solely those of the authors and do not necessarily represent those of their affiliated organizations, or those of the publisher, the editors and the reviewers. Any product that may be evaluated in this article, or claim that may be made by its manufacturer, is not guaranteed or endorsed by the publisher.

Supplementary material

The Supplementary Material for this article can be found online at: <https://www.frontiersin.org/articles/10.3389/fonc.2022.967982/full#supplementary-material>

References

1. Razumilava N, Gores GJ. Cholangiocarcinoma. *Lancet (London England)* (2014) 383:2168–79. doi: 10.1016/S0140-6736(13)61903-0
2. Siegel RL, Miller KD, Fuchs HE, Jemal A. Cancer statistics, 2022. *CA Cancer J Clin* (2022) 72:7–33. doi: 10.3322/caac.21708
3. Peery AF, Crockett SD, Murphy CC, Lund JL, Dellon ES, Williams JL, et al. Burden and cost of gastrointestinal, liver, and pancreatic diseases in the united states: Update 2018. *Gastroenterology* (2019) 156:254–272.e11. doi: 10.1053/j.gastro.2018.08.063
4. Primrose JN, Fox RP, Palmer DH, Malik HZ, Prasad R, Mirza D, et al. Capecitabine compared with observation in resected biliary tract cancer (BILCAP): A randomised, controlled, multicentre, phase 3 study. *Lancet Oncol* (2019) 20:663–73. doi: 10.1016/S1470-2045(18)30915-X
5. Brown ZJ, Hewitt DB, Pawlik TM. Biomarkers of intrahepatic cholangiocarcinoma: Diagnosis and response to therapy. *Front Biosci - Landmark* (2022) 27:85. doi: 10.31083/j.fbl2703085
6. Rizvi S, Gores GJ. Emerging molecular therapeutic targets for cholangiocarcinoma. *J Hepatol* (2017) 67:632–44. doi: 10.1016/j.jhep.2017.03.026
7. Mavros MN, Economopoulos KP, Alexiou VG, Pawlik TM. Treatment and prognosis for patients with intrahepatic cholangiocarcinoma: Systematic review and meta-analysis. *JAMA Surg* (2014) 149:565–74. doi: 10.1001/jamasurg.2013.5137
8. Chen X, Du J, Huang J, Zeng Y, Yuan K. Neoadjuvant and adjuvant therapy in intrahepatic cholangiocarcinoma. *J Clin Transl Hepatol* (2022) 10:553–63. doi: 10.14218/JCTH.2021.00250

9. Kim RD, Chung V, Alese OB, El-Rayes BF, Li D, Al-Toubah TE, et al. A phase 2 multi-institutional study of nivolumab for patients with advanced refractory biliary tract cancer. *JAMA Oncol* (2020) 6:888–94. doi: 10.1001/jamaoncol.2020.0930
10. Kurebayashi Y, Kubota N, Sakamoto M. Immune microenvironment of hepatocellular carcinoma, intrahepatic cholangiocarcinoma and liver metastasis of colorectal adenocarcinoma: Relationship with histopathological and molecular classifications. *Hepatol Res* (2021) 51:5–18. doi: 10.1111/hepr.13539
11. Louis C, Edeline J, Coulouarn C. Targeting the tumor microenvironment in cholangiocarcinoma: implications for therapy. *Expert Opin Ther Targets* (2021) 25:153–62. doi: 10.1080/14728222.2021.1882998
12. Zhang M, Yang H, Wan L, Wang Z, Wang H, Ge C, et al. Single-cell transcriptomic architecture and intercellular crosstalk of human intrahepatic cholangiocarcinoma. *J Hepatol* (2020) 73:1118–30. doi: 10.1016/j.jhep.2020.05.039
13. Banales JM, Marin JGG, Lamarca A, Rodrigues PM, Khan SA, Roberts LR, et al. Cholangiocarcinoma 2020: The next horizon in mechanisms and management. *Nat Rev Gastroenterol Hepatol* (2020) 17:557–88. doi: 10.1038/s41575-020-0310-z
14. Su M, Qiao K-Y, Xie X-L, Zhu X-Y, Gao F-L, Li C-J, et al. Development of a prognostic signature based on single-cell RNA sequencing data of immune cells in intrahepatic cholangiocarcinoma. *Front Genet* (2021) 11:615680. doi: 10.3389/fgene.2020.615680
15. Li W, Guo R, Song Y, Jiang Z. Erythroblastic island macrophages shape normal erythropoiesis and drive associated disorders in erythroid hematopoietic diseases. *Front Cell Dev Biol* (2021) 8:613885. doi: 10.3389/fcell.2020.613885
16. Bian Z, Gong Y, Huang T, Lee CZW, Bian L, Bai Z, et al. Deciphering human macrophage development at single-cell resolution. *Nature* (2020) 582:571–6. doi: 10.1038/s41586-020-2316-7
17. Li W, Wang Y, Chen L, An X. Erythroblast island macrophages: Recent discovery and future perspectives. *Blood Sci* (2019) 1:61–4. doi: 10.1097/b9.0000000000000017
18. Li W, Wang Y, Zhao H, Zhang H, Xu Y, Wang S, et al. Identification and transcriptome analysis of erythroblastic island macrophages. *Blood* (2019) 134:480–91. doi: 10.1182/blood.2019000430
19. Wynn TA, Chawla A, Pollard JW. Macrophage biology in development, homeostasis and disease. *Nature* (2013) 496:445–55. doi: 10.1038/nature12034
20. Guo R, Lü M, Cao F, Wu G, Gao F, Pang H, et al. Single-cell map of diverse immune phenotypes in the acute myeloid leukemia microenvironment. *biomark Res* (2021) 9:15. doi: 10.1186/s40364-021-00265-0
21. Cao W, Fan W, Wang F, Zhang Y, Wu G, Shi X, et al. GM-CSF impairs erythropoiesis by disrupting erythroblastic island formation via macrophages. *J Transl Med* (2022) 20:11. doi: 10.1186/s12967-021-03214-5
22. Wang Y, Li W, Schulz VP, Zhao H, Qu X, Qi Q, et al. Impairment of human terminal erythroid differentiation by histone deacetylase 5 deficiency. *Blood* (2021) 138:1615–27. doi: 10.1182/blood.2020007401
23. Zhou S-L, Xin H-Y, Sun R-Q, Zhou Z-J, Hu Z-Q, Luo C-B, et al. Association of KRAS variant subtypes with survival and recurrence in patients with surgically treated intrahepatic cholangiocarcinoma. *JAMA Surg* (2022) 157:59–65. doi: 10.1001/jamasurg.2021.5679
24. Paro A, Hyer JM, Pawlik TM. The impact of tumor burden on survival differs by morphological subtype among patients diagnosed with intrahepatic cholangiocarcinoma. *J Gastrointest Surg* (2022). doi: 10.1007/s11605-022-05329-6
25. Yang H, Yan M, Li W, Xu L. SIRP α and PD1 expression on tumor-associated macrophage predict prognosis of intrahepatic cholangiocarcinoma. *J Transl Med* (2022) 20:140. doi: 10.1186/s12967-022-03342-6
26. Li W, Li T, Sun C, Du Y, Chen L, Du C, et al. Identification and prognostic analysis of biomarkers to predict the progression of pancreatic cancer patients. *Mol Med* (2022) 28:43. doi: 10.1186/s10020-022-00467-8
27. Li W, Xu L, Wang Y, Zhao L, Kellner DB, Gao Q. Efficacy of tumor-infiltrating lymphocytes combined with IFN- α in Chinese resected stage III malignant melanoma. *J Immunol Res* (2017) 2017:1092507. doi: 10.1155/2017/1092507
28. Mazières J, Brugger W, Cappuzzo F, Middel P, Frosch A, Bara I, et al. Evaluation of EGFR protein expression by immunohistochemistry using h-score and the magnification rule: Re-analysis of the SATURN study. *Lung Cancer* (2013) 82:231–7. doi: 10.1016/j.lungcan.2013.07.016
29. Yu G, Wang LG, Han Y, He QY. ClusterProfiler: An R package for comparing biological themes among gene clusters. *Omi A J Integr Biol* (2012) 16:284–7. doi: 10.1089/omi.2011.0118
30. Jiang P, Gu S, Pan D, Fu J, Sahu A, Hu X, et al. Signatures of T cell dysfunction and exclusion predict cancer immunotherapy response. *Nat Med* (2018) 24:1550–8. doi: 10.1038/s41591-018-0136-1
31. Zhang Z, Liu F, Chen W, Liao Z, Zhang W, Zhang B, et al. The importance of N6-methyladenosine modification in tumor immunity and immunotherapy. *Exp Hematol Oncol* (2022) 11:30. doi: 10.1186/s40164-022-00281-2
32. Fabris L, Perugorria MJ, Mertens J, Björkström NK, Cramer T, Lleo A, et al. The tumour microenvironment and immune milieu of cholangiocarcinoma. *Liver Int Off J Int Assoc Study Liver* (2019) 39 Suppl 1:63–78. doi: 10.1111/liv.14098
33. Paillet J, Kroemer G, Pol JG. Immune contexture of cholangiocarcinoma. *Curr Opin Gastroenterol* (2020) 36:70–6. doi: 10.1097/MOG.0000000000000613
34. Chen Z, Yu M, Yan J, Guo L, Zhang B, Liu S, et al. PNOX expressed by b cells in cholangiocarcinoma was survival related and LAIR2 could be a T cell exhaustion biomarker in tumor microenvironment: Characterization of immune microenvironment combining single-cell and bulk sequencing technology. *Front Immunol* (2021) 12:647209. doi: 10.3389/fimmu.2021.647209
35. Zhu S, Yi M, Wu Y, Dong B, Wu K. Roles of tumor-associated macrophages in tumor progression: implications on therapeutic strategies. *Exp Hematol Oncol* (2021) 10:60. doi: 10.1186/s40164-021-00252-z
36. Wang L, He T, Liu J, Tai J, Wang B, Chen Z, et al. Pan-cancer analysis reveals tumor-associated macrophage communication in the tumor microenvironment. *Exp Hematol Oncol* (2021) 10:31. doi: 10.1186/s40164-021-00226-1
37. Zavidij O, Haradhvala NJ, Mouhieddine TH, Sklavenitis-Pistofidis R, Cai S, Reidy M, et al. Single-cell RNA sequencing reveals compromised immune microenvironment in precursor stages of multiple myeloma. *Nat Cancer* (2020) 1:493–506. doi: 10.1038/s43018-020-0053-3
38. Xiang X, Wang J, Lu D, Xu X. Targeting tumor-associated macrophages to synergize tumor immunotherapy. *Signal Transduct Target Ther* (2021) 6:75. doi: 10.1038/s41392-021-00484-9
39. Pittet MJ, Michielin O, Migliorini D. Clinical relevance of tumour-associated macrophages. *Nat Rev Clin Oncol* (2022) 19:402–21. doi: 10.1038/s41571-022-00620-6
40. Ren MH, Chen S, Wang LG, Rui WX, Li P. LINC00941 promotes progression of non-small cell lung cancer by sponging miR-877-3p to regulate VEGFA expression. *Front Oncol* (2021) 11:650037. doi: 10.3389/fonc.2021.650037
41. Li M, Li S, Zhou L, Yang L, Wu X, Tang B, et al. Immune infiltration of MMP14 in pan cancer and its prognostic effect on tumors. *Front Oncol* (2021) 11:717606. doi: 10.3389/fonc.2021.717606
42. Li X, Li K, Li M, Lin X, Mei Y, Huang X, et al. Chemoresistance transmission via exosome-transferred MMP14 in pancreatic cancer. *Front Oncol* (2022) 12:844648. doi: 10.3389/fonc.2022.844648
43. Jost M, Folgueras AR, Frérart F, Pendas AM, Blacher S, Houard X, et al. Earlier onset of tumoral angiogenesis in matrix metalloproteinase-19-deficient mice. *Cancer Res* (2006) 66:5234–41. doi: 10.1158/0008-5472.CAN-05-4315
44. Han F, Zhang L, Liao S, Zhang Y, Qian L, Hou F, et al. The interaction between S100A2 and KPNA2 mediates NFYA nuclear import and is a novel therapeutic target for colorectal cancer metastasis. *Oncogene* (2022) 41:657–70. doi: 10.1038/s41388-021-02116-6
45. Chen Y-C, Pohl G, Wang T-L, Morin PJ, Risberg B, Kristensen GB, et al. Apolipoprotein e is required for cell proliferation and survival in ovarian cancer. *Cancer Res* (2005) 65:331–7. doi: 10.1158/0008-5472.331.65.1
46. Yim M-S, Ha Y-S, Kim IY, Yun S-J, Choi YH, Kim W-J. HMOX1 is an important prognostic indicator of nonmuscle invasive bladder cancer recurrence and progression. *J Urol* (2011) 185:701–5. doi: 10.1016/j.juro.2010.09.081
47. Chen J, Zhong MC, Guo H, Davidson D, Mishel S, Lu Y, et al. SLAMF7 is critical for phagocytosis of haematopoietic tumour cells via mac-1 integrin. *Nature* (2017) 544:493–7. doi: 10.1038/nature22076
48. Nagahara M, Mimori K, Kataoka A, Ishii H, Tanaka F, Nakagawa T, et al. Correlated expression of CD47 and SIRPA in bone marrow and in peripheral blood predicts recurrence in breast cancer patients. *Clin Cancer Res* (2010) 16:4625–35. doi: 10.1158/1078-0432.CCR-10-0349
49. Datar I, Sanmamed MF, Wang J, Henick BS, Choi J, Badri T, et al. Expression analysis and significance of PD-1, LAG-3, and TIM-3 in human non-small cell lung cancer using spatially resolved and multiparametric single-cell analysis. *Clin Cancer Res* (2019) 25:4663–73. doi: 10.1158/1078-0432.CCR-18-4142
50. Terme M, Ullrich E, Aymeric L, Meinhardt K, Desbois M, Delahaye N, et al. IL-18 induces PD-1-dependent immunosuppression in cancer. *Cancer Res* (2011) 71:5393–9. doi: 10.1158/0008-5472.CAN-11-0993
51. Gottlieb AB, Krueger JG. HLA region genes and immune activation in the pathogenesis of psoriasis. *Arch Dermatol* (1990) 126:1083–6. doi: 10.1001/archderm.1990.01670320107021
52. Fernandes-Alnemri T, Yu J-W, Datta P, Wu J, Alnemri ES. AIM2 activates the inflammasome and cell death in response to cytoplasmic DNA. *Nature* (2009) 458:509–13. doi: 10.1038/nature07710
53. Kumar A, Humphreys TD, Kremer KN, Bramati PS, Bradfield L, Edgar CE, et al. CXCR4 physically associates with the T cell receptor to signal in T cells. *Immunity* (2006) 25:213–24. doi: 10.1016/j.immuni.2006.06.015
54. Förster R, Schubel A, Breitfeld D, Kremmer E, Renner-Müller I, Wolf E, et al. CCR7 coordinates the primary immune response by establishing functional

microenvironments in secondary lymphoid organs. *Cell* (1999) 99:23–33. doi: 10.1016/S0092-8674(00)80059-8

55. Emgård J, Kammoun H, Garcia-Cassani B, Chesné J, Parigi SM, Jacob J-M, et al. Oxysterol sensing through the receptor GPR183 promotes the lymphoid-Tissue-Inducing function of innate lymphoid cells and colonic inflammation. *Immunity* (2018) 48:120–132.e8. doi: 10.1016/j.immuni.2017.11.020

56. Kim S-H, Han S-Y, Azam T, Yoon D-Y, Dinarello CA. Interleukin-32: A cytokine and inducer of TNF α . *Immunity* (2005) 22:131–42. doi: 10.1016/j.immuni.2004.12.003

57. Bhat H, Zaun G, Hamdan TA, Lang J, Adomati T, Schmitz R, et al. Arenavirus induced CCL5 expression causes NK cell-mediated melanoma regression. *Front Immunol* (2020) 11:1849. doi: 10.3389/fimmu.2020.01849

58. Glass WG, Sarisky RT, Del Vecchio AM. Not-so-sweet sixteen: the role of IL-16 in infectious and immune-mediated inflammatory diseases. *J Interf Cytokine Res Off J Int Soc Interf Cytokine Res* (2006) 26:511–20. doi: 10.1089/jir.2006.26.511

59. Papadopoulos KP, Gluck L, Martin LP, Olszanski AJ, Tolcher AW, Ngarmchamnanrith G, et al. First-in-human study of AMG 820, a monoclonal anti-colony-stimulating factor 1 receptor antibody, in patients with advanced solid tumors. *Clin Cancer Res* (2017) 23:5703–10. doi: 10.1158/1078-0432.CCR-16-3261

60. Petrova PS, Viller NN, Wong M, Pang X, Lin GHY, Dodge K, et al. TTI-621 (SIRP α Fc): A CD47-blocking innate immune checkpoint inhibitor with broad antitumor activity and minimal erythrocyte binding. *Clin Cancer Res* (2017) 23:1068–79. doi: 10.1158/1078-0432.CCR-16-1700

61. O'Connell P, Hyslop S, Blake MK, Godbehere S, Amalfitano A, Aldhamen YA. SLAMF7 signaling reprograms T cells toward exhaustion in the tumor microenvironment. *J Immunol* (2021) 206:193–205. doi: 10.4049/jimmunol.2000300

62. Lai W-CV, Feldman DL, Buonocore DJ, Brzostowski EB, Rizvi H, Plodkowski AJ, et al. PD-L1 expression, tumor mutation burden and response to

immune checkpoint blockade in patients with HER2-mutant lung cancers. *J Clin Oncol* (2018) 36:9060. doi: 10.1200/JCO.2018.36.15_suppl.9060

63. Wang Z, Duan J, Cai S, Han M, Dong H, Zhao J, et al. Assessment of blood tumor mutational burden as a potential biomarker for immunotherapy in patients with non-small cell lung cancer with use of a next-generation sequencing cancer gene panel. *JAMA Oncol* (2019) 5:696–702. doi: 10.1001/jamaoncol.2018.7098

64. Serpas V, Rogers JE, Xiao L, Mola-Rudd K, Dasari A, Kee BK, et al. Impact of antibiotic exposure on the efficacy of immune checkpoint blockade in MSI-h metastatic CRC. *J Clin Oncol* (2020) 38:161. doi: 10.1200/JCO.2020.38.4_suppl.161

65. Iyer G, Audenet F, Middha S, Carlo MI, Regazzi AM, Funt S, et al. Mismatch repair (MMR) detection in urothelial carcinoma (UC) and correlation with immune checkpoint blockade (ICB) response. *J Clin Oncol* (2017) 35:4511. doi: 10.1200/JCO.2017.35.15_suppl.4511

66. Lança T, Silva-Santos B. The split nature of tumor-infiltrating leukocytes: Implications for cancer surveillance and immunotherapy. *Oncoimmunology* (2012) 1:717–25. doi: 10.4161/onci.20068

67. Loo Yau H, Ettayebi I, De Carvalho DD. The cancer epigenome: Exploiting its vulnerabilities for immunotherapy. *Trends Cell Biol* (2019) 29:31–43. doi: 10.1016/j.tcb.2018.07.006

68. Jiang Z, Sun H, Yu J, Tian W, Song Y. Targeting CD47 for cancer immunotherapy. *J Hematol Oncol* (2021) 14:180. doi: 10.1186/s13045-021-01197-w

69. Sun M, Qi J, Zheng W, Song L, Jiang B, Wang Z, et al. Preliminary results of a first-in-human phase I study of IMM01, SIRP α fc protein in patients with relapsed or refractory lymphoma. *J Clin Oncol* (2021) 39:2550–0. doi: 10.1200/jco.2021.39.15_suppl.2550

70. Gordon SR, Maute RL, Dulken BW, Hutter G, George BM, McCracken MN, et al. PD-1 expression by tumour-associated macrophages inhibits phagocytosis and tumour immunity. *Nature* (2017) 545:495–9. doi: 10.1038/nature22396